

Modulation Technique of Localized Surface Plasmon Resonance of Palladium Nanospheres by Coating with Titanium Dioxide Shell for Application to Photothermal Therapy Agent

Yutaro Hayakawa

Nihon University

Masato Furuya

Nihon University

Hironobu Tahara

Nagasaki University

Yasuhiro Kosuge

Nihon University

Tsuyoshi Kimura

Tokyo Medical and Dental University

Kosuke Sugawa (✉ sugawa.kosuke@nihon-u.ac.jp)

Nihon University

Joe Otsuki

Nihon University

Research Article

Keywords: Localized surface plasmon resonance, Palladium nanospheres, Photothermal therapy, Photothermal conversion, Titanium dioxide

Posted Date: March 31st, 2022

DOI: <https://doi.org/10.21203/rs.3.rs-1462233/v1>

License:  This work is licensed under a Creative Commons Attribution 4.0 International License.

[Read Full License](#)

Abstract

Although plasmonic palladium (Pd) nanospheres are thermodynamically stable and have high photothermal conversion due to the free and bound electron coupling associated with the intrinsic high interband transition, they have not attracted attention as a photothermal conversion material for next-generation photothermal cancer therapy. This is because the Pd nanospheres generate the localized surface plasmon resonance (LSPR) intrinsically in the ultraviolet region, which is far away from the biological transparent window (750–900 nm). In this study, we controlled the LSP wavelength of Pd nanospheres by coating with high refractive index TiO₂ shells taking advantage of the Pd LSPR which is highly sensitive to changes in the local refractive index around the nanospheres. Our calculations indicated that the absorption cross-section at 808 nm (corresponding to the wavelength used for photothermal treatment) was increased by 2.8 times by red-shifting the LSPR and increasing the extinction intensity associated with the coating with TiO₂ shell. Experiments confirmed the theoretical prediction in that the LSPR of the synthesized Pd nanospheres with a diameter of 81 nm was significantly red-shifted by coating with amorphous TiO₂ shell, resulting in significant large extinction intensity at 808 nm. The photothermal conversion efficiency was estimated to be 50%. *In vitro* cell tests, HeLa cells incubated with 100–300 µg/mL TiO₂-coated Pd nanospheres were efficiently killed by irradiating 808 nm laser (1.8 W) even though the nanospheres with the same concentrations showed little cytotoxicity. These results indicate that the Pd nanospheres coated with high refractive index shells can be promising as a photothermal therapy agent.

Introduction

Localized surface plasmon resonance (LSPR) of metal nanoparticles has been one of the most important optical phenomena for the development of photothermal therapy techniques as a next-generation noninvasive cancer therapy[1–5]. To maximize the useful effects of LSPR in the technology, to control the wavelength and intensity of LSPR is important. The LSPR of metal nanoparticles incorporated near the tumor region is excited by irradiating laser light in the near-infrared region (biological transparent window: 750–900 nm) where the penetration depth into bio-tissues is large[6]. The strong local heat generated during the deactivation of the LSPR leads to the death of cancer cells. Therefore, the metal nanoparticles of which a strong LSPR can be generated in the biological transparent window must be developed. Although the gold (Au) nanoparticles with high chemical stability in biological environments are considered one of the most useful plasmonic photothermal therapy agents, Au nanospheres generally show an LSPR at approximately 500 nm, which is much shorter than the biological transparent window. To tune the LSPR of Au toward the biological transparent window, anisotropic Au nanoparticles have been developed intensely, including Au nanorods[5], Au nanostars[7], Au nanoprisms[8], and so on. However, the morphology of these nanoparticles is intrinsically thermodynamically unstable. In addition, cetyltrimethylammonium bromide, which is often required as a protective agent to realize the morphological anisotropy[9–12], has a high cytotoxicity[13, 14]; complete removal of the surfactant is

still difficult[15–21]. In short, an alternative approach is desired for tuning the LSPR wavelength to the biological transparent window.

Palladium (Pd) nanoparticles are one of the plasmonic metal nanomaterials having a high imaginary part of dielectric function derived from the intrinsic interband transition across a wide UV-visible-near infrared region[22, 23]. Therefore, the Pd nanoparticles may have a high photothermal conversion efficiency through the enhanced formation of excited electron-hole pairs by the coupling between the free- and bound-electron response of palladium[24]. In addition, Pd nanoparticles have an intrinsically high chemical stability in the biological environments. However, the usefulness of Pd nanospheres as a photothermal therapeutic material is considered to be limited since they generate the LSPR only in the UV region. Consequently, the application of Pd LSPR to photothermal conversion is limited to only a few examples[25–27] while attention to anisotropic Pd nanoparticles have been increasing recently. We recently found that the LSPR wavelength of Pd nanospheres is more sensitive to a change in the refractive index of their surrounding environment, as compared with Au and Ag nanospheres[28]. This is attributed to the small wavelength dispersion of real part of the Pd dielectric function. This finding prompted us to consider an expectation that the LSPR wavelength of Pd nanospheres could be significantly red-shifted by hybridization with a high refractive index material. In this study, the useful optical specificity as a photothermal therapy agent of the Pd nanosphere, which are coated with a high refractive index semiconductor, was theoretically demonstrated through the comparison with a bare Pd nanosphere and general Au nanosphere coated with the semiconductor. Our experiments corroborated the theoretical calculations; the LSPR wavelength of synthesized Pd nanospheres was significantly red-shifted by coating with a titanium dioxide (TiO_2) shell, resulting in a significant increase in the extinction intensity at 808 nm, which corresponds to the laser wavelength used for the photothermal therapeutic treatment. It has been further demonstrated in this study that the Pd nanospheres coated with TiO_2 shells show a low cytotoxicity and efficient photothermal therapeutic performance *in vitro*.

Methods

Materials.

Deionized water (resistivity: 18.2 MW cm^{-1}), which was obtained from a Milli-Q water purification system, was utilized for the preparation of all aqueous solutions. Hydrogen tetrachloroaurate(III) tetrahydrate ($\text{HAuCl}_4 \cdot 4\text{H}_2\text{O}$, Nacalai Tesque), trisodium citrate dihydrate (Kanto Chemical, Japan), L-ascorbic acid (Fujifilm Wako Pure Chemical, Japan), palladium(II) chloride (PdCl_2 , Fujifilm Wako Pure Chemical, Japan), hydrochloric acid (HCl, Fujifilm Wako Pure Chemical, Japan), hydroxypropyl cellulose (Sigma-Aldrich, United States), 2-propanol (Kishida Chemical, Japan), ammonium aqueous solution (28 wt.%, Kishida Chemical, Japan), titanium diisopropoxide bis(acetylacetonate) (TDAA, Sigma-Aldrich, United States), and 8-ArmPEG-Amine (20,000 Da, Biopharma PEG Scientific, United States), were used as received. Dulbecco's Modified Eagle's Medium (D-MEM, low glucose) with L-glutamine and phenol red, and PBS(-) were obtained from Fujifilm Wako Pure Chemical, Japan. Penicillin streptomycin, trypsin-EDTA

(0.25%), and fetal bovine serum (FBS) were obtained from Gibco, United States. HeLa cell lines were purchased from JCRB Cell Bank, Japan.

Synthesis of Au(core)/Pd(shell) nanoparticles (Au/PdNSs, Step 1 and 2 in Scheme 1).

Small spherical Au nanoparticles were synthesized using a citric acid reduction method[29]. After an aqueous solution (1 wt%, 4 mL) of citric acid was added to an aqueous solution (0.01 wt%, 100 mL) of $\text{HAuCl}_4 \cdot 4\text{H}_2\text{O}$, which was refluxed for 30 min in advance, the mixed solution was further refluxed for 1 hour, resulting in the formation of spherical Au nanoparticles.

The Au/PdNSs were synthesized as follows[28,30]. An aqueous solution of hydrogen tetrachloropalladate (II) ($\text{H}_2\text{Pd}_4\text{Cl}_4$, 1 mM, 100 mL) was prepared by dissolving PdCl_2 (17.7 mg) in an aqueous solution of hydrochloric acid (1 mM, 100 mL). Next, the colloidal aqueous solution of spherical Au nanoparticles (2.5 mL) was added into the aqueous solution of hydrogen tetrachloropalladate (II) (100 mL). Then, an aqueous solution (20 mL) containing of ascorbic acid (60 mM) and the citrate (0.1 wt.%) was slowly added dropwise into the mixed solution under stirring in an ice bath. After the addition was finished, the mixed solution was further stirred for 30 min in an ice bath, resulting in the formation of Au/PdNSs. The Au/PdNSs was purified by the centrifugation (12,000 rpm, 10 min), followed by redispersing in an aqueous solution of citric acid (0.1 wt.%, 25 mL).

Coating Au/PdNSs with TiO_2 shell (Au/PdNSs/ TiO_2 , Step 3 in Scheme 1).

The coating of Au/PdNSs with TiO_2 shell (Au/PdNSs/ TiO_2) was performed using a modified version of the previous report[31]. First, an aqueous solution of hydroxypropyl cellulose (0.5 wt.%, 360 mL) was added into the colloidal aqueous solution of Au/PdNSs (9 mL), followed by stirring the solution for 1 h. Next, after 2-propanol (36 mL) and ammonium aqueous solution (28%, 1 mL) were added to the mixed colloidal solution, a 2-propanol solution of TDAA (10 mM, 225 mL) was slowly added dropwise to the solution every hour three times under stirring, followed by stirring for 20 h, resulting in the formation of Au/PdNSs/ TiO_2 . The obtained Au/PdNSs/ TiO_2 was purified by the centrifugation (12,000 rpm, 10 min) once, followed by redispersing in ethanol (10 mL). Finally, after the colloidal solution was diluted 10 times by ethanol, the solution was refluxed at 100 °C for 5 h.

Modification of eight-arm PEG amine on Au/PdNSs/ TiO_2 (Step 4 in Scheme 1)

The eight-arm PEG amine was modified onto Au/PdNSs/ TiO_2 by adding an ethanol solution of eight-arm PEG amine (10 mg/mL, 1 mL) into the colloidal ethanol solution of Au/PdNSs/ TiO_2 (1 mL), followed by stirring for 1 h. The colloidal solution was purified by the centrifugation (12,000 rpm, 10 min), followed by redispersing in Milli-Q water (1 mL).

Measurements

The extinction spectra of resultant colloidal solution were measured using a V-770 spectrophotometer (JASCO). For the evaluation of the photothermal conversion properties of Au/PdNSs/TiO₂ modified with 8-arm PEG amine, the temperature of the colloidal aqueous solution (2 mL) was measured using a thermocouple (OMEGA HW206) inserted in the solution under gentle stirring in a standard 1 cm quartz cell. A continuous wave (CW) laser with 808 nm (1.8 W) was applied to the colloidal solution. The distance between the laser source and surface of the cell was set to be 10 cm. Time variation of the temperature under the laser irradiation was measured up to arbitrary period, whereof the temperature of the colloidal solution reached a saturated state. Transmission electron microscopy (TEM) image was taken with a Hitachi HF-2000 with an acceleration voltage of 200 kV. The extinction, absorption, and scattering spectra of Au/PdNSs/TiO₂ were calculated by analytical Mie theory using MatScat program on MATLAB[32,33]. The Mie series was truncated by the Bohren-Huffman treatment[34] and the dielectric function of Pd and TiO₂ were used from the previous reports[22,35].

Evaluation of Cytotoxicity and Photothermal Therapeutic Effect of Au/PdNSs/TiO₂

HeLa cell lines were cultured in D-MEM containing 1% penicillin/streptomycin and 10% FBS at 37 °C under 5% CO₂. For the evaluation of cytotoxicity and photothermal therapeutic effect of Au/PdNSs/TiO₂, HeLa cells (2.0 × 10⁴ cells/well, 700 mL) were seeded in four well plates and incubated for 24 h to allow the cells to attach to the bottom surface of the well. The colloidal aqueous solutions of Au/PdNSs/TiO₂ modified with 8-arm PEG amine were centrifuged (10,000 rpm, 10 min) and redispersed in PBS (100 mL). After the addition of D-MEM (200 mL) into the PBS of Au/PdNSs/TiO₂, the mixed solutions were added to the respective wells (concentrations: 100, 200, and 300 µg/mL). After incubating the cells with Au/PdNSs/TiO₂ for 3 h and at 37 °C under 5% CO₂, the medium containing the Au/PdNSs/TiO₂ was removed. The D-MEM (700 mL) containing calcein AM (1 µM) and PI (0.5 µM), which selectively label the live and dead cells with green and red fluorescence, respectively, was added to the each well, followed by incubating for 20 min at 37 °C under 5% CO₂, and then the D-MEM was removed from the well. The cell observation was performed using a BX53 fluorescence microscope (Olympus). To evaluate the photothermal therapeutic effect, after incubating the cells with Au/PdNSs/TiO₂ (concentrations: 100, 200, and 300 µg/mL) for 3 h at 37 °C under 5% CO₂, the cells were exposed to a CW laser (808 nm, 1.8 W) for 5 min. After removing the medium from these systems, the cells, which were labeled with calcein AM and PI, were observed. The cell viability was determined by calculating the percentage of calcein-positive cells to the total number of cells.

Results And Discussion

Theoretical optical properties of Pd nanosphere coated with TiO₂ shell.

We previously showed that the optical spectra of Au/PdNS core/shell particles can be approximated by those of homogeneous Pd nanospheres when the Au core is small enough. Therefore, we used Pd nanosphere as models for experimental Au/PdNS in the calculations. The optical characteristics of a Pd

nanosphere (PdNS) which is coated with TiO₂ shell (PdNS/TiO₂) were compared with a bare PdNS and a spherical Au nanoparticle (AuNS) coated with TiO₂ (AuNS/TiO₂). The geometric models (Figure 1(A)) of PdNS and PdNS/TiO₂ were employed from the morphology of experimentally-obtained Au/PdNS and Au/PdNS/TiO₂ (*vide infra*). The properties of LSPR of metal nanoparticles can be described by the Mie theory, which gives analytical and exact solutions of the Maxwell equations for spherical nanoparticles with the multipole expansion of the electromagnetic fields[34]. In the extinction spectrum ((a) in Figure 1(B)) of PdNS with a diameter of 81 nm simulated on the basis of the Mie theory, a broad extinction band attributed to the dipole mode of Pd LSPR was observed at 407 nm in the visible region. The band was extended to the biological transparent window including 808 nm, which corresponds to the laser wavelength used for *in vitro* photothermal therapeutic performance. The extinction cross-section at 808 nm was $2.54 \times 10^3 \text{ nm}^2$ (Figure 1(D)). The coating with TiO₂ with the thickness of 28 nm on PdNS red-shifted the band by 137 nm, resulting in the maximum extinction wavelength at 544 nm ((a) in Figure 1(B)). The large red-shift is due to the inherently great refractive index sensitivity of Pd LSPR[28]; the refractive index of amorphous TiO₂ ($n = 2.54$ at 407 nm) is significantly higher than that ($n = 1.333$) of surrounding water. Note that the extinction cross-section at 808 nm of Pd LSPR was increased by 3.1 times ($8.00 \times 10^3 \text{ nm}^2$) as shown in Figure 1(D). Next, the fraction of absorption component in the extinction at 808 nm should be considered because the deactivation process of LSP resonance can be divided into absorption (nonradiative decay), which directly contributes to the photothermal conversion, and scattering (radiative decay). The extinction, absorption, and scattering spectra for PdNS and PdNS/TiO₂ are shown in (b) and (c) in Figure 1(B), respectively. For both nanoparticles, although the absorption cross-section is slightly larger than that of scattering cross-section around the maximum extinction wavelengths, the absorption cross-section becomes dominant at the longer wavelengths (PdNS: 71% and PdNS/TiO₂: 62% for absorption/extinction ratio at 808 nm). The higher absorption/extinction ratios, compared to spherical Au nanoparticles (*vide infra*), are due to the effective coupling between the free- and bound-electron response of Pd. Consequently, the absorption cross-section ($5.00 \times 10^3 \text{ nm}^2$) of PdNS/TiO₂ was approximately 2.8 times higher than that ($1.81 \times 10^3 \text{ nm}^2$) of PdNS (Figure 1(E)).

Next, the results of PdNS and PdNS/TiO₂ are compared with AuNS and AuNS/TiO₂, respectively, with the same geometries. As shown in (a) in Figure 1(C), the maximum extinction wavelength of LSP resonance of AuNS was red-shifted by 95 nm by coating with the TiO₂ shell. The magnitude of the red-shift was smaller than that for PdNS because the refractive index sensitivity of AuNS was smaller than that of PdNS[28]. The LSP resonance bands of both AuNS (558 nm) and AuNS/TiO₂ (653 nm) exhibited their maximum at longer wavelengths than those of PdNS and PdNS/TiO₂. However, the bands of Au nanospheres are significantly sharper than those of Pd nanospheres, and consequently, the absorption cross-sections of Au nanospheres is smaller than those of Pd nanospheres at 808 nm (Figure 1(E)). Particularly, the absorption cross-section of AuNS/TiO₂ was 60% lower than that of PdNS/TiO₂. These results suggest that the PdNS/TiO₂ would have a superior performance as a photothermal treatment material than PdNS, AuNS, and AuNS/TiO₂.

Morphological and optical characterization of Au/PdNSs/TiO₂

We previously shown that the LSP resonance wavelength of PdNS (dipole mode) is longer for larger particles and was in near ultraviolet to visible region at with diameters above 40 nm[28]. On the other hand, the nanoparticles of which the diameter is too large (> 100 nm) can lead to the reduced dispersion stability in an aqueous phase. Therefore, we synthesized PdNSs with a diameter of approximately 80 nm. These Au/PdNSs were synthesized by seed-mediated growth method using small spherical Au nanoparticles (average diameter: 13.7 ± 1.9 nm, Figure S1) as a core because the PdNSs with precisely controlled diameters have been successfully prepared by this method. Figure 2(A) shows the TEM image of Au/PdNSs and the size distribution calculated from the multiple similar TEM images. It was confirmed that Au/PdNSs formed a spherical shape with rugged surface. The highest abundance of nanoparticles was in the range of 75-79 nm and the average diameter was 81.0 ± 7.5 nm. The Au/PdNSs were coated with the shell of TiO₂ (Au/PdNSs/TiO₂) as a high refractive index semiconductor, because TiO₂ nanomaterials are well known to show high biocompatibility[36,37]. The TEM image confirmed that the Au/PdNSs was coated by the TiO₂ shell ((a) in Figure 2(B)). The size distribution of Au/PdNSs/TiO₂ ((b) in Figure 2(B)) was relatively broad over 125-149 nm and the average diameter was 136.9 ± 9.6 nm. Therefore, the thickness of TiO₂ shell was estimated to be approximately 28 nm. Any peaks attributed to the crystalline TiO₂ were not observed in the XRD spectrum of Au/PdNSs/TiO₂ (Figure 2(C)), which indicate that the coating TiO₂ is amorphous, while the diffraction peaks of crystalline palladium, which matched with the data of Joint Committee on Powder Diffraction Standards (JCPDS), were observed[31].

The optical spectra of the synthesized Au/PdNSs/TiO₂ are shown in Figure 3. The extinction spectrum of the colloidal aqueous solution of small Au nanoparticles (core only) showed an LSP resonance peak at 525 nm. On the other hand, in the colloidal aqueous solution of Au/PdNSs, no Au-derived band was observed; instead, a broad extinction band with the maximum at 360 nm derived from the Pd LSP resonance was observed. This is consistent with our previous results that the LSP resonance of Au nanoparticle cores was completely shielded by the thick Pd shell (Figure S2)[28]. Therefore, our synthesized Au/PdNSs can be optically treated as a PdNSs. Next, the maximum extinction wavelength of the LSP resonance of Au/PdNSs/TiO₂ was 468 nm, which was red-shifted by 108 nm compared to that of Au/PdNSs. This large red-shift, which is attributed to the increase in the surrounding refractive index by coating with TiO₂ shell, was qualitatively consistent with the calculated results as shown in (a) of Figure 1(B), although the magnitude of the red-shift was somewhat smaller than the calculated value (137 nm) and the obtained resonance band was broader. The overestimation of the red-shift by calculation for the TiO₂-coated nanoparticles may be derived from the difference between the calculated (407 nm) and observed (360 nm) LSPR peak values for the Pd cores, which may be further amplified by incorporating the high refractive index shell because the refractive index sensitivity increases with wavelength[28]. On the other hand, the broader observed LSPR band may be attributed to the wide distribution of experimental TiO₂ shell thickness (shown in (b) in Figure 2(B)). In any case, the red-shifted and broad

LSPR extending to the near-IR region implied that Au/PdNS/TiO₂ could be a useful photothermal therapy agent, particularly because of the high extinction intensity at 808 nm.

Photothermal conversion properties of Au/PdNSs/TiO₂

To investigate the photothermal conversion properties of Au/PdNSs/TiO₂, temperature changes induced by the irradiation of 808 nm laser (1.8 W) to the colloidal aqueous solution (extinction intensity at 808 nm: 0.33) was measured (Figure 4(A)). The irradiation to the colloidal aqueous solution resulted in the temperature rise as much as 20.3 °C, while pure water showed only a 2.8 °C increase under the same irradiation conditions. The photothermal conversion efficiency (η) were calculated using Equation 1 according to the method developed in previous reports[38,39]

$$\eta = \frac{hS(T_{\max} - T_{\text{surr}}) - Q_{\text{dis}}}{I(1 - 10^{-A})} \quad \text{Equation 1}$$

where h and S are the heat transfer coefficient and the surface area of the 1 cm quartz cell as a container. The T_{\max} and T_{surr} are the maximum steady-state temperature and the temperature of the surrounding environment, respectively. The Q_{dis} represents the heat generated by pure water under the irradiation of 808 nm laser as shown in Figure 4(A). The lumped quantity hS is estimated using Equation 2.

$$\tau_s = \frac{\sum_i m_i C_{p,i}}{hS} \quad \text{Equation 2}$$

where τ_s , m_i , and $C_{p,i}$ are the system time constant, mass of water ($m_{\text{H}_2\text{O}}$) and quartz cell (m_{cell}), and heat capacities of water ($C_{p,\text{H}_2\text{O}}$: 4.2 J/g) and quartz cell ($C_{p,\text{cell}}$: 0.839 J/g)[40]. As presented in Figure 4(B), the τ_s value is estimated by fitting the cooling temperature profiles to Equations 3 and 4.

$$t = -\tau_s \ln \theta \quad \text{Equation 3}$$

$$\theta = \frac{T - T_{\text{surr}}}{T_{\max} - T_{\text{surr}}} \quad \text{Equation 4}$$

where t and θ are the cooling time and dimensionless driving force temperature, respectively. The T is the temperature of the system at time t . Consequently, the h was calculated to be 50 %. Although the value was somewhat lower than the ratio of absorption in the extinction components (62%), this may be due to an increase in the scattering component owing to the rugged surface of Au/PdNSs ((a) in Figure 2(A)). However, this value is higher than those of reported anisotropic Au nanoparticles in studies as a photothermal therapy agent: Au nanorods: 21%[41], Au nanocages: 28%[42], and Au nanoshells: 25%[43], which suggests that Au/PdNSs/TiO₂ can function as a superior photothermal therapy agent. Further, it

was found that Au/PdNSs/TiO₂ is stable optically, and hence morphologically as well, against laser irradiation, which is demonstrated by only a minor difference in the extinction spectra before and after the laser irradiation as shown in Figure 4(C).

In vitro evaluation of biocompatibility and photothermal therapeutic ability of Au/PdNSs/TiO₂

The photothermal therapeutic ability of Au/PdNSs/TiO₂ under the irradiation of 808 nm laser was investigated *in vitro*. For the application of Au/PdNSs/TiO₂, the eight-arm PEG amine was modified on Au/PdNSs/TiO₂ for efficient uptake into the cells and improved dispersion stability in PBS[44]. First, the cytotoxicity of Au/PdNSs/TiO₂ was investigated under dark conditions using HeLa cells. The cytotoxicity evaluated by co-staining the live and dead cells with calcein AM and propidium iodide (PI), respectively. The cell viability was calculated using the Equation 5:

Cell viability

$$= \frac{\text{Number of cells stained with calcein AM}}{\text{Total number of cells stained with both calcein AM and PI}} \quad \text{Equation 5}$$

Appropriate application of Equation 5 requires that the total number of cells is more or less the same in each well. That this condition was met is shown by the counting data (concentration of Au/PdNSs/TiO₂, total number of cells): 0 mg/mL, 95 ± 8 mm⁻²; 100 mg/mL, 99 ± 22 mm⁻²; 200 mg/mL, 118 ± 26 mm⁻²; and 300 mg/mL, 114 ± 8 mm⁻². As shown in Figure 5(A) and (C), the viability of cells incubated with Au/PdNSs/TiO₂ for all concentrations was high (> 98%), which was similar to that (98.1 ± 1.1%) obtained without the nanoparticles. Next, with irradiation with 808 nm laser, the cellular viability was decreased with the increasing concentration of Au/PdNSs/TiO₂ with the lowest viability being 1.8% at the highest concentration (300 mg/mL) as shown in Figure 5(B) and (C). Since the laser irradiation to the cells without Au/PdNSs/TiO₂ did not reduce the cell viability (100.0 ± 0.0%), the large decrease in the cellular viability was attributed to the photothermal therapeutic effect of Au/PdNSs/TiO₂, demonstrating that the Au/PdNSs/TiO₂ functioned as a photothermal therapy agent.

Conclusion

In this study, the authors focused on the control technique of the resonance wavelength of PdNSs utilizing a high refractive index sensitivity of Pd LSPR. It was theoretically and experimentally demonstrated that the LSPR was red-shifted from ultraviolet to visible region by coating with TiO₂ shell. In addition, it was theoretically found that the absorption cross-section at 808 nm, which governs the photothermal conversion ability, was largely improved by the red-shifting. It was demonstrated from the experimental *in-vitro* cell tests that the death of HeLa cells was induced by exciting the LSPR of PdNSs associated with the laser (808 nm) irradiation. These results suggest that hybridization of PdNSs with high refractive index TiO₂ was important for improving the photothermal therapeutic effect. Furthermore,

we surmise that combining with materials with even higher refractive indices could further improve the photothermal therapeutic effect of PdNSs. Currently, we are proceeding with research according to the strategy.

Abbreviations

LSPR: Localized surface plasmon resonance, PdNS: Palladium nanospheres, Au/PdNSs: Au(core)/Pd(shell) nanospheres, PdNS/TiO₂: Palladium nanospheres coated with TiO₂ shell, Au/PdNSs/TiO₂: Au(core)/Pd(shell) nanospheres coated with TiO₂ shell, Au: Gold, Pd: Palladium.

Declarations

Competing interests

The authors declare that they have no competing interests.

Availability of Data and Materials

The datasets used or analyzed during the current study are available from the corresponding author on reasonable request.

Acknowledgement

The authors would like to thank KM for his experimental assistance.

Authors' Contributions

KS and JO initiated and supervised the study. HT carried out and supervised the spectral calculation of metal nanoparticles. YH carried out the experiments. MF performed data analysis. YK and TK guided the experiments and data analysis. KS, JO, YH, HT co-wrote the paper. All authors read and approved the final manuscript.

Funding

This work was supported by the JSPS KAKENHI grant, number 19H05627 and 20H02850.

Author details

¹Department of Materials and Applied Chemistry, College of Science and Technology, Nihon University, Chiyoda, Tokyo 101-8308, Japan

²Graduate School of Engineering, Nagasaki University, Bunkyo, Nagasaki, 852-8521, Japan

³Laboratory of Pharmacology, School of Pharmacy, Nihon University, 7-7-1 Narashinodai, Chiba, Funabashi 274-8555, Japan

⁴Institute of Biomaterials and Bioengineering, Tokyo Medical and Dental University, Chiyoda, Tokyo 101-0062, Japan

Consent for publication

The author and all co-authors agree to publish.

Ethics approval and consent to participate

Not applicable.

References

1. Lv Z, He S, Wang Y, Zhu X (2021) Noble Metal Nanomaterials for NIR-Triggered Photothermal Therapy in Cancer. *Adv Healthc Mater* 10(6): 2001806.
2. Sztandera K, Gorzkiewicz M, Klajnert-Maculewicz B (2019) Gold Nanoparticles in Cancer Treatment. *Mol Pharm* 16(1): 1–23. <https://doi.org/10.1021/acs.molpharmaceut.8b00810>
3. Lal S, Clare SE, Halas NJ (2008) Nanoshell-Enabled Photothermal Cancer Therapy: Impending Clinical Impact. *Acc Chem Res* 41(12): 1842–1851. <https://doi.org/10.1021/ar800150g>
4. Link S, El-Sayed MA (2000) Shape and size dependence of radiative, non-radiative and photothermal properties of gold nanocrystals. *Int Rev Phys Chem* 19(3): 409–453. <https://doi.org/10.1080/01442350050034180>
5. Huang X, El-Sayed IH, Qian W, El-Sayed MA (2006) Cancer Cell Imaging and Photothermal Therapy in the Near-Infrared Region by Using Gold Nanorods. *J Am Chem Soc* 128(6): 2115–2120. <https://doi.org/10.1021/ja057254a>
6. Hemmer E, Benayas A, Legare F, Vetrone F (2016) Exploiting the biological windows: current perspectives on fluorescent bioprobes emitting above 1000 nm. *Nanoscale Horiz* 1(3): 168–184. <https://doi.org/10.1039/C5NH00073D>
7. Yuan H, Fales AM, Vo-Dinh T (2012) TAT Peptide-Functionalized Gold Nanostars: Enhanced Intracellular Delivery and Efficient NIR Photothermal Therapy Using Ultralow Irradiance. *J Am Chem Soc* 134(28): 11358–11361. <https://doi.org/10.1021/ja304180y>
8. Perez-Hernandez M, del Pino P, Mitchell SG, Moros, M, Stepien, G, Pelaz, B, Parak, WJ, Galvez, EM, Pardo, J, de la Fuente JM (2015) Dissecting the Molecular Mechanism of Apoptosis during Photothermal Therapy Using Gold Nanoprisms. *ACS Nano* 9(1): 52–61. <https://doi.org/10.1021/nn505468v>
9. Nikoobakht B, El-Sayed MA (2003) Preparation and growth mechanism of gold nanorods (NRs) using seed-mediated growth method. *Chem Mater* 15(10): 1957–1962.

<https://doi.org/10.1021/cm020732l>

10. Sau TK, Murphy CJ (2004) Room temperature, high-yield synthesis of multiple shapes of gold nanoparticles in aqueous solution. *J Am Chem Soc* 126(28): 8648–8649.
<https://doi.org/10.1021/ja047846d>
11. Millstone JE, Park S, Shuford KL, Qin L, Schatz, GC, Mirkin CA (2005) Observation of a Quadrupole Plasmon Mode for a Colloidal Solution of Gold Nanoprisms. *J Am Chem Soc* 127(15): 5312–5313.
<https://doi.org/10.1021/ja043245a>
12. Murphy CJ, Sau TK, Gole AM, Orendorff CJ, Gao J, Gou L, Hunyadi SE, Li T (2005) Anisotropic metal nanoparticles: synthesis, assembly, and optical applications. *Journal of Physical Chemistry B* 109(29): 13857–13870. <https://doi.org/10.1021/jp0516846>
13. Alkilany AM, Murphy CJ (2010) Toxicity and cellular uptake of gold nanoparticles: what we have learned so far? *J Nanopart Res* 12(7): 2313–2333. <https://doi.org/10.1007/s11051-010-9911-8>
14. Alkilany AM, Nalaria PK, Hexel CR, Shaw TJ, Murphy CJ, Wyatt MD (2009) Cellular uptake and cytotoxicity of gold nanorods: molecular origin of cytotoxicity and surface effects. *Small* 5(6): 701–708. <https://doi.org/10.1002/smll.200801546>
15. Burrows ND, Lin W, Hinman, Joshua G, Dennison, JM, Vartanian AM, Abadeer NS, Grzincic EM, Jacob LM, Li J, Murphy, CJ (2016) Surface Chemistry of Gold Nanorods. *Langmuir* 32(39): 9905–9921.
<https://doi.org/10.1021/acs.langmuir.6b02706>
16. Wan J, Wang J-H, Liu T, Xie Z, Yu X-F, Li W (2015) Surface chemistry but not aspect ratio mediates the biological toxicity of gold nanorods in vitro and in vivo. *Sci. Rep* 5: 11398.
<https://doi.org/10.1038/srep11398>
17. Takahashi H, Niidome Y, Niidome T, Kaneko K, Kawasaki H, Yamada S (2006) Modification of Gold Nanorods Using Phosphatidylcholine to Reduce Cytotoxicity. *Langmuir* 22(1): 2–5.
<https://doi.org/10.1021/la0520029>
18. Wang J, Dong B, Chen B, Xu S, Zhang S, Yu W, Xu C, Song H (2013) Glutathione modified gold nanorods with excellent biocompatibility and weak protein adsorption, targeting imaging and therapy toward tumor cells. *Dalton Trans* 42(32): 11548–11558. <https://doi.org/10.1039/C3DT51246K>
19. Mehtala JG, Zemlyanov DY, Max JP, Kadasala N, Zhao S, Wei A (2014) Citrate-Stabilized Gold Nanorods. *Langmuir* 30(46): 13727–13730. <https://doi.org/10.1021/la5029542>
20. Liu K, Zheng Y, Lu Xun, Thai T, Lee NA, Bach U, Gooding JJ (2015) Biocompatible Gold Nanorods: One-Step Surface Functionalization, Highly Colloidal Stability, and Low Cytotoxicity. *Langmuir* 31(17): 4973–4980. <https://doi.org/10.1021/acs.langmuir.5b00666>
21. Nishida K, Kawasaki H (2017) Effective removal of surface-bound cetyltrimethylammonium ions from thiol-monolayer-protected Au nanorods by treatment with dimethyl sulfoxide/citric acid. *RSC Adv* 7(29): 18041–18045. <https://doi.org/10.1039/C7RA02179H>
22. Pakizeh T, Langhammer C, Zoric I, Apell P, Kall M (2009) Intrinsic Fano Interference of Localized Plasmons in Pd Nanoparticles. *Nano Lett* 9(2): 882–886. <https://doi.org/10.1039/C7RA02179H>

23. Langhammer C, Yuan Z, Zoric I, Kasemo B (2006) Plasmonic Properties of Supported Pt and Pd Nanostructures. *Nano Lett* 6(4): 833–838. <https://doi.org/10.1021/nl803794h>
24. Zoric I, Zaech M, Kasemo B, Langhammer C (2011) Gold, Platinum, and Aluminum Nanodisk Plasmons: Material Independence, Subradiance, and Damping Mechanisms. *ACS Nano* 5(4): 2535–2546. <https://doi.org/10.1021/nn102166t>
25. Huang X, Tang S, Mu X, Dai Y, Chen G, Zhou Z, Ruan F, Yang Z, Zheng N (2011) Freestanding palladium nanosheets with plasmonic and catalytic properties. *Nat Nanotechnol* 6(1): 28–32. <https://doi.org/10.1038/nnano.2010.235>
26. Tang S, Chen M, Zheng N (2014) Sub-10-nm Pd nanosheets with renal clearance for efficient near-infrared photothermal cancer therapy. *Small* 10(15): 3139–3144. <https://doi.org/10.1002/smll.201303631>
27. Liu Y, Ding L, Wang D, Lin M, Sun H, Zhang H, Sun H, Yang B (2018) Hollow Pd Nanospheres Conjugated with Ce6 To Simultaneously Realize Photodynamic and Photothermal Therapy. *ACS Appl Bio Mater* 1(4): 1102–1108. <https://doi.org/10.1021/acsabm.8b00318>
28. Sugawa K, Tahara H, Yamashita A, Otsuki J, Sagara T, Harumoto T, Yanagida S (2015) Refractive Index Susceptibility of the Plasmonic Palladium Nanoparticle: Potential as the Third Plasmonic Sensing Material. *ACS Nano* 9(2): 1895–1904. <https://doi.org/10.1021/nn506800a>
29. Turkevich J, Stevenson PC, Hillier J (1951) The nucleation and growth processes in the synthesis of colloidal gold. *Discuss Faraday Soc* 11: 55–75. <https://doi.org/10.1039/DF9511100055>
30. Hu J-W, Zhang Y, Li J-F, Liu Z, Ren B, Sun S-G, Tian Z-Q, Lian, T (2005) Synthesis of Au@Pd core-shell nanoparticles with controllable size and their application in surface-enhanced Raman spectroscopy. *Chem Phys Lett* 408(4–6): 354–359. <https://doi.org/10.1016/j.cplett.2005.04.071>
31. Seh ZW, Liu S, Low M, Zhang SY, Liu Z, Mlayah A, Han M-Y (2012) Janus Au-TiO₂ Photocatalysts with Strong Localization of Plasmonic Near-Fields for Efficient Visible-Light Hydrogen Generation. *Adv Mater* 24(17): 2310–2314. <https://doi.org/10.1002/adma.201104241>
32. Schäfer, J.-P., Implementierung und Anwendung analytischer und numerischer Verfahren zur Lösung der Maxwellgleichungen für die Untersuchung der Lichtausbreitung in biologischem Gewebe, PhD thesis, Universität Ulm, 2011, <http://vts.uni-ulm.de/doc.asp?id=7663>.
33. Schäfer J, Lee S-C, Kienle, A (2012) Calculation of the near fields for the scattering of electromagnetic waves by multiple infinite cylinders at perpendicular incidence. *J Quant Spectrosc Radiat Transfer* 113(16): 2113–2123. <https://doi.org/10.1016/j.jqsrt.2012.05.019>
34. Bohren CF and Huffman DR *Absorption and Scattering of Light by Small Particles*, Wiley, New York, 1983.
35. Dakhel AA (2003) Structural and optical properties of evaporated Zn oxide, Ti oxide and Zn-Ti oxide films. *Appl Phys A* 77(5): 677–682. <https://doi.org/10.1007/s00339-002-1763-3>
36. Han W, Wang YD, Zheng, YF (2008) In vitro biocompatibility study of nano TiO₂ materials. *Adv Mat Res* 47–50(Pt. 2): 1438–1441. <https://doi.org/10.4028/www.scientific.net/AMR.47-50.1438>

37. Han W, Wang Y, Zheng Y In vivo biocompatibility studies of nano TiO₂ materials. *Adv Mat Res* 79–82(Pt. 1): 389–392. <https://doi.org/10.4028/www.scientific.net/AMR.79-82.389>
38. Roper DK, Ahn W, Hoepfner M (2007) Microscale Heat Transfer Transduced by Surface Plasmon Resonant Gold Nanoparticles. *J Phys Chem C* 111(9): 3636–3641. <https://doi.org/10.1021/jp064341w>
39. Tian Q, Jiang F, Zou R, Liu Q, Chen Z, Zhu M, Yang S, Wang J, Wang J, Hu J (2011) Hydrophilic Cu₉S₅ Nanocrystals: A Photothermal Agent with a 25.7% Heat Conversion Efficiency for Photothermal Ablation of Cancer Cells in Vivo. *ACS Nano* 5(12): 9761–9771. <https://doi.org/10.1021/nn203293t>
40. Liu P, Yang W, Shi L, Zhang H, Xu Y, Wang P, Zhang G, Chen WR, Zhang B, Wang X, Concurrent photothermal therapy and photodynamic therapy for cutaneous squamous cell carcinoma by gold nanoclusters under a single NIR laser irradiation. *J Mater Chem B* 7(44): 6924–6933. <https://doi.org/10.1039/C9TB01573F>
41. Li Z, Huang H, Tang S, Li Y, Yu X-F, Wang H, Li P, Sun Z, Zhang H, Liu C, Chu PK (2016) Small gold nanorods laden macrophages for enhanced tumor coverage in photothermal therapy. *Biomaterials* 74: 144–154. <https://doi.org/10.1016/j.biomaterials.2015.09.038>
42. Zeng J, Goldfeld D, Xia Y (2013) A Plasmon-Assisted Optofluidic (PAOF) System for Measuring the Photothermal Conversion Efficiencies of Gold Nanostructures and Controlling an Electrical Switch. *Angew Chem Int Ed* 52(15): 4169–4173. <https://doi.org/10.1002/anie.201210359>
43. Pattani VP, Tunnell JW (2012) Nanoparticle-mediated photothermal therapy: a comparative study of heating for different particle types. *Lasers Surg Med* 44(8): 675–684. <https://doi.org/10.1002/lsm.22072>
44. Tian Y, Luo S, Yan H, Teng Z, Pan Y, Zeng L, Wu J, Li Y, Liu Y, Wang S, Lu G (2015) Gold nanostars functionalized with amine-terminated PEG for X-ray/CT imaging and photothermal therapy. *J Mater Chem B* 3(21): 4330–4337. <https://doi.org/10.1039/C5TB00509D>
45. Rakic AD, Djuricic AB, Elazar JM, Majewski ML (1998) Optical properties of metallic films for vertical-cavity optoelectronic devices. *Appl Opt* 37(22); 5271–5283. <https://doi.org/10.1364/AO.37.005271>

Scheme

Scheme 1 is available in supplementary section.

Figures

Figure 1

Optical properties of PdNS, PdNS/TiO₂, AuNS and AuNS/TiO₂ calculated by the Mie theory. Dielectric function of Pd[22] and Au[45] were taken from the previous papers. Refractive index of TiO₂[35] was taken from the previous paper. (A) geometrical model of PdNS/TiO₂ for the calculation. (B) (a) extinction spectra for PdNS and PdNS/TiO₂ and extinction, absorption, and scattering spectra for (b) PdNS and (c) PdNS/TiO₂. (C) (a) extinction spectra for AuNS and AuNS/TiO₂ and extinction, absorption, and scattering spectra for (b) AuNS and (c) AuNS/TiO₂. (D) Extinction and (E) absorption cross-sections of PdNS, PdNS/TiO₂, AuNS and AuNS/TiO₂.

Figure 2

Morphological characterization of Au/PdNSs and Au/PdNSs/TiO₂. (a) TEM image and (b) size distribution for (A) Au/PdNSs and (B) Au/PdNSs/TiO₂. (C) (a) XRD patterns of Au/PdNSs/TiO₂ and (b) JCPDS data of palladium.

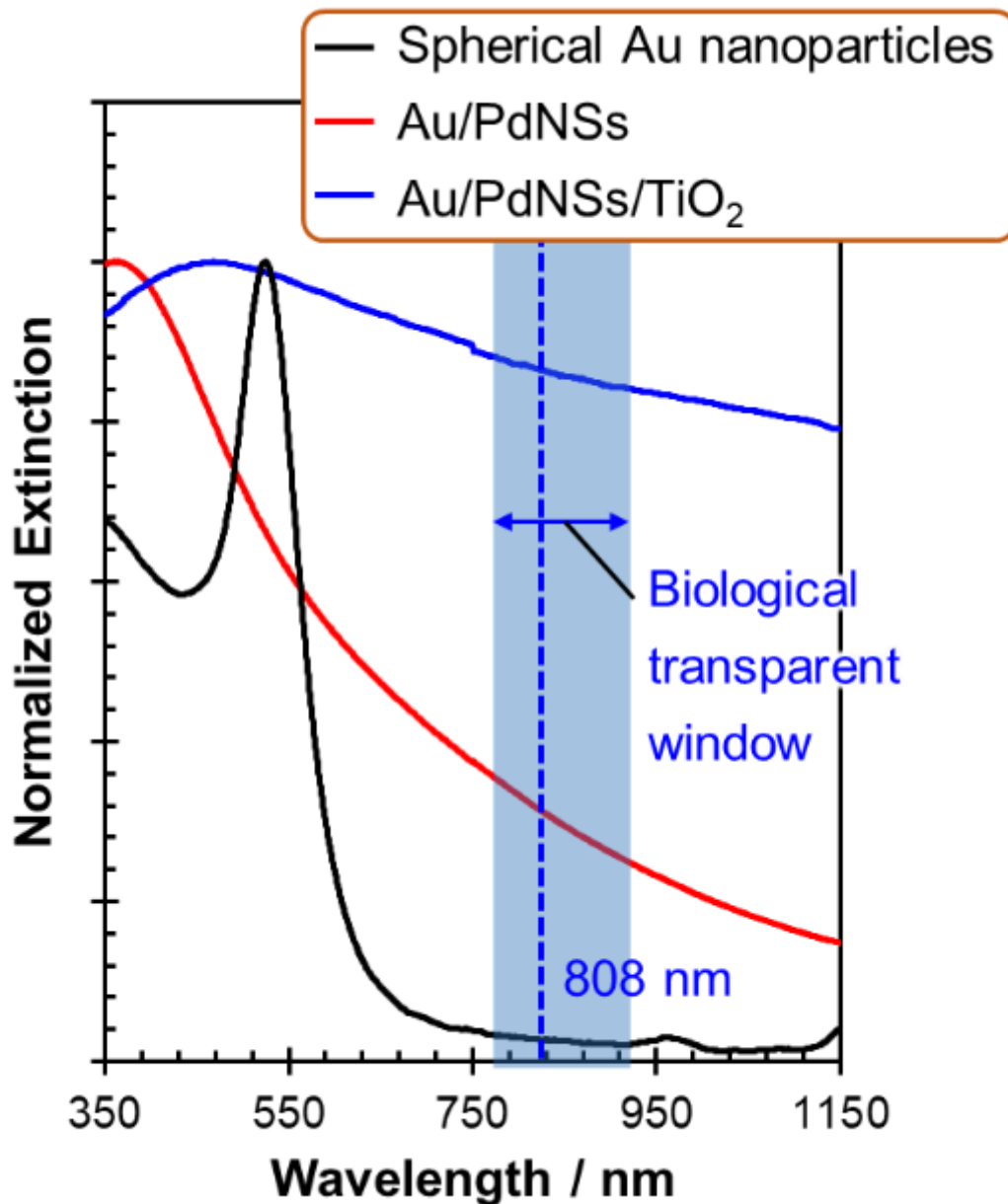


Figure 3

Extinction spectra of colloidal aqueous solutions of spherical Au nanoparticles, Au/PdNSs and Au/PdNSs/TiO₂.

Figure 4

Photothermal conversion properties and stability against laser irradiation of Au/PdNSs/TiO₂. (A) Temperature profiles of colloidal aqueous solution of Au/PdNSs/TiO₂ and water as a reference under laser irradiation with 808 nm. (B) Time constant for heat transfer from the system was calculated by applying the linear time data from the cooling period *versus* negative natural logarithm of driving force

temperature, which obtained from (A). (C) Extinction spectra for Au/PdNSs/TiO₂ before and after the laser irradiation.

Figure 5

Cell viability after incubating HeLa cells with Au/PdNSs/TiO₂. (A) Fluorescence images of calcein AM and PI-co-stained HeLa cells, which were incubated (a) without and with the concentrations of (b) 100, (c) 200, and (c) 300 mg/mL Au/PdNSs/TiO₂. (B) Fluorescence images of calcein AM and PI-co-stained HeLa cells, which were incubated (a) without and with the concentrations of (b) 100, (c) 200, and (c) 300 mg/mL Au/PdNSs/TiO₂, after laser irradiation with 808 nm (1.5 W). The scale bars of all images equal to 100 μm. (C) Quantitative cell viability obtained from respective conditions of (A) and (B).

Supplementary Files

This is a list of supplementary files associated with this preprint. Click to download.

- [220317AuPdNSsTiO2SI.pdf](#)
- [floatimage1.png](#)